OTFS-IM with Decode and Forward Relaying

Vighnesh S Bhat and A. Chockalingam
Department of ECE, Indian Institute of Science, Bangalore 560012

***Abstract*—Orthogonal time frequency space (OTFS) modulation and index modulation (IM) are promising techniques in wireless communications. OTFS excels in high mobility scenarios by using information signaling in the delay-Doppler domain, while IM offers improved spectral efficiencies and bit error performance. In this study, we analyze the performance of OTFS with IM (OTFS-IM) in a decode-and-forward (DaF) relay communication system. The communication involves two hops between the transmitter, receiver nodes through a relay node. We derive a closed-form expression for the end-to-end pairwise error probability in OTFS-IM with DaF relaying and assess the achieved asymptotic diversity order. Our simulation results show that *i*) the use of indexing improves the performance of OTFS with DaF relaying *ii*) the simulated upper bound on the bit error rate (BER) validates the analytically predicted diversity orders.**

***Index Terms*—OTFS modulation, index modulation, decode and forward relaying, pairwise error probability, diversity analysis.**

I. Introduction

As mobile communications demand higher frequencies and faster speeds, dealing with rapidly changing channels with strong Doppler effects becomes a challenge. To overcome this, orthogonal time frequency space (OTFS) modulation has been proposed in recent literature, which is known for its ability to provide robust performance in high-Doppler channels [1]. OTFS modulation uniquely offers information symbol multiplexing in the delay-Doppler (DD) domain, making it an appealing solution in this context.

The existing literature on OTFS explores diverse aspects such as low-complexity signal detection, DD channel estimation, peak-to-average power ratio, pulse shaping, and multiple access [2]-[5]. Studies have analyzed OTFS performance, including diversity analysis for uncoded single-input single-output OTFS [6], achieving full diversity with phase rotation (PR) [6], and investigating diversity orders for multiple-input multiple-output OTFS (MIMO-OTFS) [6] and space-time coded OTFS (STC-OTFS) [8]. Additionally, coded OTFS has been studied, revealing a trade-off between coding gain and diversity gain [9].

In light of the increasing spectral efficiency demands for 5G and beyond wireless networks, index modulation (IM) techniques have emerged as a promising solution. IM allows the transmission of additional information bits through indexing of various transmission entities, such as transmit antennas and time slots. When applied to multicarrier systems like OTFS, IM has shown improvements in spectral efficiency and overall performance [10]. Studies have demonstrated that OTFS with IM (OTFS-IM) outperforms traditional orthogonal frequency division multiplexing (OFDM) with indexing [10]. The work in [11] showed that the diversity and peak-to-average power ratio (PAPR) of OTFS are improved using indexing. In [12], a dual mode indexing scheme in OTFS and a minimum Hamming distance based log-likelihood ratio detector are reported. In [13], an enhanced IM scheme in OTFS that exploited the in-phase and quadrature dimensions for improved spectral efficiency is reported.

Cooperative relaying is a widely recognized means to enhance the range and coverage in wireless communications [14], [15]. Amplify-and-forward (AaF) and decode-and-forward (DaF) protocols are widely studied owing to their simplicity and practicality. Single-relay and multi-relay schemes without and with relay selection have been investigated in a variety of system settings [16]-[18]. Previous studies [17]-[18] have investigated the impact of node mobility on cooperative communication, highlighting its potential for performance degradation. However, this issue can be mitigated by leveraging the inherent robustness of OTFS in cooperative communications. Consequently, there is a growing interest in understanding the performance of OTFS in relaying systems under high-mobility conditions. In the recent literature, authors have analyzed the performance of OTFS with DaF relaying in the context of OTFS-based downlink LEO satellite communication, focusing on outage analysis for the ideal bi-orthogonal pulse [19]. The incorporation of IM techniques in cooperative communication systems further enhances energy efficiency, spectral efficiency, and extends coverage, making relay-assisted communication an attractive paradigm to overcome the limitations of traditional point-to-point OTFS systems. In this regard we present an analysis of the end-to-end performance of OTFS-IM in DaF relaying systems. Our novel contributions in this paper are as follows.

- We derive a closed-form expression for the end-to-end pairwise error probability (PEP) of OTFS-IM with DaF relaying, considering rectangular pulses and fractional DD profiles and characterize the achieved asymptotic diversity order.
- We also analyze the system when phase rotation (PR) of OTFS frames is employed to achieve improved diversity performance.
- Simulation results show that 1) the use of indexing enhances the performance of OTFS with DaF relaying, and 2) the simulated upper bound on the BER validates the analytically derived diversity orders for OTFS-IM with DaF relaying.

This work was supported by the J. C. Bose National Fellowship, Department of Science and Technology, Government of India.

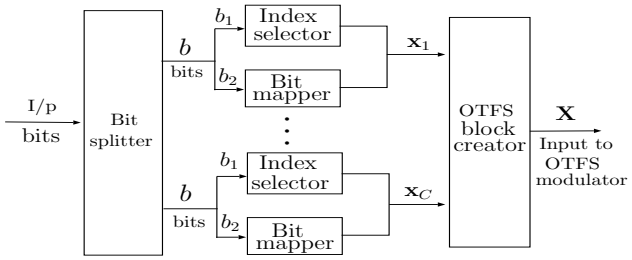

Fig. 1: Delay-Doppler indexing.

The paper is organized as follows. In Sec. II, we introduce the OTFS-IM model considered for DaF relaying. Sec. III presents the performance analysis of this system. The numerical results and discussions are provided in Sec. IV. Finally, Sec. V provides a summary of our conclusions.

Notations: Matrices are denoted by uppercase boldface letters, while vectors are represented by lowercase boldface letters. A diagonal matrix with elements $\{x_1, x_2, \ldots, x_n\}$ is expressed as $\text{diag}\{x_1, x_2, \ldots, x_n\}$. The Frobenius norm of a matrix $\mathbf{X}$ is indicated as $|\mathbf{X}|$. An N point IDFT matrix is denoted by $\mathbf{F}_N$ and identity matrix of size N by $\mathbf{I}_N$. Transposition, Hermitian, and conjugation operations are denoted by $(\cdot)^T$, $(\cdot)^H$, and $(\cdot)^*$, respectively. A complex Gaussian distribution with mean μ and variance σ^2 is represented by $\mathcal{CN}(\mu, \sigma^2)$. The expectation operation is denoted by $\mathbb{E}[\cdot]$. The symbol $|.|$ denotes the absolute value of a number or the cardinality of a set.

II. System model

In this section, we present the OTFS-IM scheme. This scheme utilizes two elements to carry information. Complex symbols from a modulation alphabet, which are multiplexed within the DD grid, and the indexing of DD bins in the grid. The DD grid, comprising a total of MN DD bins, is of size $M \times N$, where M and N represent the number of delay and Doppler bins, respectively. This grid constitutes one OTFS frame.

A. DD indexing in OTFS

The DD grid is partitioned into sub-blocks (SBs) to support indexing. Each SB contains u number of DD bins, with v number of bins activated and $u - v$ number of DD bins are left idle. The number of SBs, denoted as C, is determined by the ratio of the total DD bins (MN) to the bins per SB (u), expressed as $C = \frac{MN}{u}$. Within an SB, a subset of DD bins, represented by v, carries active complex symbols from the modulation alphabet $\mathbb{A}$, while the remaining bins remain idle and are filled with zeros. To encode the index information for each SB, a certain number of index bits, denoted as b_1, are required, which can be computed as $\lfloor \log_2 \binom{u}{v} \rfloor$. The total number of index bits in the entire DD grid is then given by $C\lfloor \log_2 \binom{u}{v} \rfloor$. Similarly, the number of modulation bits per SB, denoted as b_2, is determined by the number of active DD bins v and the size of the modulation alphabet $|\mathbb{A}|$, expressed as $b_2 = v \log_2 |\mathbb{A}|$. Consequently, the total number of modulation bits in the grid is calculated as $Cb_2 = Cv \log_2 |\mathbb{A}|$. The overall number of modulation bits in the entire grid is given by $Cb_2 = Cv \log_2 |\mathbb{A}|$. The total number of bits, both index and modulation bits, per SB is represented as $b = b_1 + b_2$. Therefore, the total number of bits in the entire DD grid (i.e., the total number of bits per OTFS frame) can be expressed as $Cb = C[\lfloor \log_2 \binom{u}{v} \rfloor + v \log_2 |\mathbb{A}|]$. The achieved rate of OTFS-IM scheme, measured in bits per channel use (bpcu), given as

$$\eta = \frac{C}{MN}\left[\lfloor \log_2 \binom{u}{v} \rfloor + v \log_2 |\mathbb{A}|\right]. \quad (1)$$

Figure 1 illustrates the DD domain indexing which serves as input to OTFS modulator.

B. OTFS-IM system

In the OTFS-IM scheme, jth SB is denoted as $\mathbf{x}_j = [x_{j,1}, x_{j,2}, \cdots, x_{j,u}]$, where $x_{j,i} \in \mathbb{A} \cup 0$, $0 \leq j \leq C$. These SBs are combined by the OTFS block creator to form the DD domain symbol matrix $\mathbf{X}$, which serves as the input to the OTFS modulator. The OTFS modulation scheme uses a bandwidth of $M\Delta f$ and a frame duration of NT, where $\Delta f = \frac{1}{T}$ is the subcarrier spacing. The information symbols from the DD domain undergo the inverse symplectic finite Fourier transform (ISFFT) operation, followed by the Heisenberg transform with a transmission pulse ($\mathbf{P}_{tx}$), resulting in the time domain OTFS signal denoted as $\mathbf{S}$ given by

$$\mathbf{S} = \mathbf{P}_{tx}\mathbf{X}\mathbf{F}_N^H, \quad (2)$$

The received time domain signal denoted as $\mathbf{r}$, we have

$$\mathbf{r} = \mathbf{H}\mathbf{s} + \mathbf{n}, \quad (3)$$

where $\mathbf{s} \triangleq \text{vec}(\mathbf{S})$, $\mathbf{H} = \sum_{i=1}^{L} h_i \mathbf{\Pi}^{\alpha_i + a_i} \mathbf{\Delta}^{\beta_i + b_i} \in \mathbb{C}^{MN \times MN}$, with $\mathbf{\Pi}$ representing the permutation matrix, and $\mathbf{\Delta} = \text{diag}[z^0, z^1, \cdots, z^{MN-1}]$ where $z = e^{\frac{j2\pi}{MN}}$, L denotes the number of DD paths, α_i, β_i are the integers denoting the delay and Doppler indices of the ith path, respectively, $a_i, b_i \in [-0.5, 0.5]$ are the corresponding fractional parts and $\mathbf{n} \in \mathbb{C}^{MN \times 1}$ denotes the noise vector.

At the receiver, the received signal $\mathbf{r}$ can be transformed into an $M \times N$ matrix $\mathbf{R}$ through devectorization. This matrix $\mathbf{R}$ is then subjected to the Wigner transform with a receive pulse ($\mathbf{P}_{rx}$) and the SFFT. Following the transforms, the representation of the received signal in the DD domain can be expressed as

$$\mathbf{Y} = \mathbf{F}_M^H(\mathbf{F}_M \mathbf{P}_{rx}\mathbf{R})\mathbf{F}_N = \mathbf{P}_{rx}\mathbf{R}\mathbf{F}_N. \quad (4)$$

By utilizing equations (2) and (3) in equation (4) and vectorizing the resulting equation, we obtain

$$\begin{aligned} \mathbf{y} &= (\mathbf{F}_N \otimes \mathbf{P}_{rx})\mathbf{H}(\mathbf{F}_N^H \otimes \mathbf{P}_{tx})\mathbf{x} + \tilde{\mathbf{n}}, \\ &= \mathbf{H}_{\text{eff}}\mathbf{x} + \tilde{\mathbf{n}}, \end{aligned} \quad (5)$$

where $\mathbf{x} \triangleq \text{vec}(\mathbf{X})$, $\mathbf{H}_{\text{eff}} \in \mathbb{C}^{MN \times MN}$ represents the effective channel matrix, $\tilde{\mathbf{n}} \triangleq (\mathbf{F}_N \otimes \mathbf{I}_M)\mathbf{n}$ represents the noise vector.

An alternate representation of input-output relation (5): We can express the input-output relation in (5) in an alternative form for analysis purposes. When considering rectangular

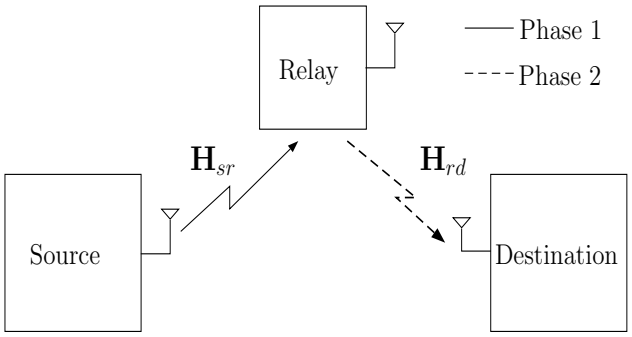

Fig. 2: OTFS-IM with decode-and-forward relaying scheme.

pulses, where $\mathbf{P}_{tx}$ and $\mathbf{P}_{rx}$ reduce to the identity matrix, the received signal vector $\mathbf{y}$ can be written as

$$\begin{aligned}\mathbf{y} &= \sum_{i=}^{L} h_i(\mathbf{F}_N \otimes \mathbf{I}_M)\mathbf{\Pi}^{\alpha_i+a_i}\mathbf{\Delta}^{\beta_i+b_i}(\mathbf{F}_N^H \otimes \mathbf{I}_M)\mathbf{x} + \tilde{\mathbf{n}}, \\ &= \mathbf{\Psi}(\mathbf{x})\mathbf{h} + \tilde{\mathbf{n}}, \end{aligned} \tag{6}$$

where $\mathbf{\Psi}(\mathbf{x}) = [\mathbf{\Xi}_1\mathbf{x}|\mathbf{\Xi}_2\mathbf{x}|\cdots|\mathbf{\Xi}_L\mathbf{x}] \in \mathbb{C}^{MN\times L}$ is a concatenated matrix with $\mathbf{\Xi}_i = (\mathbf{F}_N \otimes \mathbf{I}_M)\mathbf{\Pi}^{\alpha_i+a_i}\mathbf{\Delta}^{\beta_i+b_i}(\mathbf{F}_N^H \otimes \mathbf{I}_M)$ and $\mathbf{h} = [h_1, \cdots, h_L] \in \mathbb{C}^{L\times 1}$ is the channel vector and h_is are assumed to be i.i.d and distributed as $\mathcal{CN}(0, 1/L)$.

C. Decode-and-forward relaying with OTFS-IM

In this subsection, we introduce the system model for an OTFS-IM system with DaF relaying. Figure 2 shows the block diagram of the OTFS-IM system with DaF relaying. Due to severe signal blockage in outdoor environments, no direct link exists between the source and destination. The communication takes place in two hops, the first hop is from the source to the relay, and the second hop is from the relay to the destination. The transmission occurs in two phases. In the first phase, the source node transmits information to the relay. The received signal at the relay is given by

$$\mathbf{y}_{sr} = \mathbf{H}_{sr}\mathbf{x} + \mathbf{n}_{sr}, \tag{7}$$

where $\mathbf{y}_{sr}$ and $\mathbf{n}_{sr}$ are the received signal vector and noise vector at the relay, respectively, $\mathbf{H}_{sr}$ represents the equivalent channel matrix between the S-to-R link, and $\mathbf{x}$ is the transmit signal vector from the S.

During the second phase, the relay forwards the decoded information to the destination. The received signal at the destination, denoted as $\mathbf{y}_{rd}$, can be expressed as

$$\mathbf{y}_{rd} = \mathbf{H}_{rd}\hat{\mathbf{x}} + \mathbf{n}_{rd}, \tag{8}$$

where $\mathbf{y}_{rd}$ and $\mathbf{n}_{rd}$ are the received signal vector and noise vector at the destination, respectively, $\mathbf{H}_{rd}$ represents the equivalent channel matrix between the R-to-D link, and $\hat{\mathbf{x}}$ is the transmit signal vector from the R.

Alternate form for OTFS-IM with DaF: The input-output relation in (7) and (8) can be written in an alternate way based on (6). The received signal at the relay in the first phase can be written as

$$\begin{aligned}\mathbf{y}_{sr} &= \sum_{i=1}^{L_{sr}} h_{sr}^i(\mathbf{F}_N \otimes \mathbf{I}_M)\mathbf{\Pi}^{\alpha_i+a_i}\mathbf{\Delta}^{\beta_i+b_i}(\mathbf{F}_N^H \otimes \mathbf{I}_M)\mathbf{x} \\ &\quad + \mathbf{n}_{sr}, \\ &= \mathbf{\Psi}(\mathbf{x})\mathbf{h}_{sr} + \mathbf{n}_{sr}, \end{aligned} \tag{9}$$

Likewise, the received signal at the destination in the second phase can be written as

$$\begin{aligned}\mathbf{y}_{rd} &= \sum_{i=1}^{L_{rd}} h_{rd}^i(\mathbf{F}_N \otimes \mathbf{I}_M)\mathbf{\Pi}^{\alpha_i+a_i}\mathbf{\Delta}^{\beta_i+b_i}(\mathbf{F}_N^H \otimes \mathbf{I}_M)\hat{\mathbf{x}} \\ &\quad + \mathbf{n}_{rd}, \\ &= \mathbf{\Psi}(\hat{\mathbf{x}})\mathbf{h}_{rd} + \mathbf{n}_{rd}, \end{aligned} \tag{10}$$

where $\mathbf{h}_{sr} \in \mathbb{C}^{L_{sr}\times 1}$, $\mathbf{h}_{rd} \in \mathbb{C}^{L_{rd}\times 1}$, $\mathbf{\Psi}(\mathbf{x}) \in \mathbb{C}^{MN\times L_{sr}}$, $\mathbf{\Psi}(\hat{\mathbf{x}}) \in \mathbb{C}^{MN\times L_{rd}}$, $\mathbf{\Xi}_i$ are defined in (6), L_{sr} and L_{rd} are the number of resolvable DD domain paths between S-to-R and R-to-D links, respectively.

D. OTFS with phase rotation

Phase rotation (PR) in OTFS is performed by pre-multiplying the OTFS vector $\mathbf{x}$ by a PR matrix $\mathbf{\Theta}$, given by $\mathbf{\Theta} = \text{diag}\{e^{j\frac{q}{MN}}\}$, $q = 0, \cdots, MN-1$. Therefore, $\mathbf{x}' = \mathbf{\Theta}\mathbf{x}$ is the phase rotated OTFS transmit vector. In [6], it was shown that SISO-OTFS with the above PR operation is capable of achieving full possible diversity in the DD domain when $e^{j\frac{q}{MN}}$, $q = 0, 1, \cdots, MN-1$ are transcendental numbers and $\frac{q}{MN}$ are real, distinct, and algebraic.

III. Performance analysis

In this section, we analyze the diversity performance of OTFS-IM with DaF relaying. Maximum likelihood (ML) detection is considered at the relay and the destination. The minimum rank of difference matrices in a given system plays a key role in determining the diversity performance of the system. Therefore, we first characterize the minimum rank in the considered relaying system.

A. Minimum rank on various links with relaying

In the S-to-R link, let $\mathbf{\Psi}(\mathbf{x}_i)$ and $\mathbf{\Psi}(\mathbf{x}_j)$ be two distinct OTFS-IM symbol matrices without PR defined in (9), and $\mathbf{\Psi}(\mathbf{x}'_i)$ and $\mathbf{\Psi}(\mathbf{x}'_i)$ be two such matrices with PR. As in [6]-[7], the minimum ranks of $(\mathbf{\Psi}(\mathbf{x}_i) - \mathbf{\Psi}(\mathbf{x}_j))$ and $(\mathbf{\Psi}(\mathbf{x}'_i) - \mathbf{\Psi}(\mathbf{x}'_i))$ on the S-to-R link for OTFS-IM are $\leq L_{sr}$ and L_{sr}, respectively.

Now, consider the R-to-D link. Note that the detected vector ($\hat{\mathbf{x}}$) at the relay (error-free or erroneous) belongs to the same OTFS-IM signal set at the source. In the R-to-D link, let $\mathbf{\Psi}(\hat{\mathbf{x}}_i)$ and $\mathbf{\Psi}(\hat{\mathbf{x}}_j)$ denote two distinct symbol matrices without PR and $\mathbf{\Psi}(\hat{\mathbf{x}}'_i)$ and $\mathbf{\Psi}(\hat{\mathbf{x}}'_j)$ be two such matrices with PR. We are interested in the minimum rank of the difference matrix $(\mathbf{\Psi}(\hat{\mathbf{x}}_i) - \mathbf{\Psi}(\hat{\mathbf{x}}_j))$, $\forall i, j$. Since the detected signal vector at R, belong to the same OTFS signal set that was transmitted from source, the minimum ranks of $(\mathbf{\Psi}(\hat{\mathbf{x}}_i) - \mathbf{\Psi}(\hat{\mathbf{x}}_j))$ and $(\mathbf{\Psi}(\hat{\mathbf{x}}'_i) - \mathbf{\Psi}(\hat{\mathbf{x}}'_j))$ on the R-to-D link for the OTFS-IM are

System parameters			No. of pairs of $(\mathbf{\Psi}(\mathbf{x}_i) - \mathbf{\Psi}(\mathbf{x}_j))$ with rank					Minimum rank
				1	2	3	4	
$M = 2$, $N = 2$, $L = 2$	DD profile-1	α=[0, 1] β=[0, 0]	w/o PR	32	208	-	-	1
			with PR	0	240	-	-	2
	DD profile-2	α=[0, 1] β=[0, 1]	w/o PR	0	240	-	-	2
			with PR	0	240	-	-	2
$M = 4$, $N = 2$, $L = 2$	DD profile-3	α=[0, 1] β=[0, 0]	w/o PR	128	65152	-	-	1
			with PR	0	65280	-	-	2
	DD profile-4	α=[0, 1] β=[0, 1]	w/o PR	0	65280	-	-	2
			with PR	0	65280	-	-	2
$M = 4$, $N = 2$, $L = 4$	DD profile-5	α=[0,0,1,1] β=[0,1,0,1]	w/o PR	0	136	2072	63072	2
			with PR	0	0	0	65280	4

TABLE I: Rank profile of the difference matrices.

$\leq L_{rd}$ and L_{rd}, respectively. Table I shows the rank profiles for different DD profiles, with and without PR. For example, DD profile-1 without PR has 32 pairs with rank 1 and 208 pairs with rank 2, resulting in a minimum rank of 1 ($\leq L$). With PR, there are 240 pairs with rank 2, leading to a minimum rank of 2 (L). The DD profiles in Table I can exist in any links.

B. Diversity analysis

In this subsection, we examine the diversity performance of OTFS-IM with DaF relaying. To assess the diversity order, we establish a bound on the bit error rate using the pairwise error probability (PEP) expression. The PEP allows us to quantify the probability of error events on the S-to-R link (U) and the R-to-D link (V), denoted as $P_b(S \to R)$ and $P_b(R \to D)$, respectively. In DaF relaying, the error events U and V are independent. The intersection of these events, denoted as $W = U \cap V$, represents the errors occurring simultaneously on both links, with a probability of $P_b(S \to R)P_b(R \to D)$. At the destination, W may not contain any erroneous bits because errors in the S-to-R link can be corrected if they are also present in the R-to-D link. Consequently, we express the total end-to-end error as $U + V - (1 + \delta)W$, where δ ($0 \leq \delta \leq 1$) depends on the modulation scheme employed. In general, the probabilities $P_b(S \to R)$ and $P_b(R \to D)$ are typically small. Hence, the probability of W ($P_b(S \to R)P_b(R \to D)$) can be neglected. Consequently, the bit error probability (P_b) of the overall system can be approximated as [16]

$$P_b \approx P_b(S \to R) + P_b(R \to D). \tag{11}$$

Further, $P_b(S \to R)$ and $P_b(R \to D)$ are upper bounded by the union bound based on PEP. Assume ML detection and perfect DD channel state information at R and D. On the S-to-D link, the probability $P_b(S \to R)$ can be bounded as

$$P_b(S \to R) \leq \frac{1}{Cb\varepsilon_x} \sum_i \sum_{j,j \neq i} d_H(\mathbf{x}_i, \mathbf{x}_j) P_{SR}(\mathbf{x}_i \to \mathbf{x}_j), \tag{12}$$

where ε_x is the number of possible signal sets for $\mathbf{x}$, $d_H(\mathbf{x}_i, \mathbf{x}_j)$ is the Hamming distance between $\mathbf{x}_i$ and $\mathbf{x}_j$, and $P_{SR}(\mathbf{x}_i \to \mathbf{x}_j)$ is the average PEP between the symbol vectors $\mathbf{x}_i$ and $\mathbf{x}_j$ given by

$$P_{SR}(\mathbf{x}_i \to \mathbf{x}_j) = \mathbb{E}_{\mathbf{h}_{sr}} \left\{ Q\left(\sqrt{\frac{\|(\mathbf{\Psi}(\mathbf{x}_i) - \mathbf{\Psi}(\mathbf{x}_j))\mathbf{h}_{sr}\|^2}{2N_0}} \right) \right\}, \tag{13}$$

where the averaging is over the distribution of $\mathbf{h}_{sr}$. We have normalized the entries of $\mathbf{x}$ so that the average energy per symbol time is one and the signal-to-noise ratio (SNR) is given by $\gamma_s = 1/N_0$. Upper bounding (13) using Chernoff bound, we get

$$P_{SR}(\mathbf{x}_i \to \mathbf{x}_j) \leq \mathbb{E}_{\mathbf{h}_{sr}} \left\{ \exp\left(\frac{-\gamma_s \|(\mathbf{\Psi}(\mathbf{x}_i) - \mathbf{\Psi}(\mathbf{x}_j))\mathbf{h}_{sr}\|^2}{4} \right) \right\}, \tag{14}$$

Carrying out the averaging, we get [6]

$$P_{SR}(\mathbf{x}_i \to \mathbf{x}_j) \leq \left(\frac{1}{\prod_{l=1}^{r_{sr}} (1 + \frac{\gamma_s \lambda_{sr}^{lij}}{4L_{sr}})} \right), \tag{15}$$

where r_{sr} and λ_{sr}^{lij} are the rank and eigenvalue of $(\mathbf{\Psi}(\mathbf{x}_i) - \mathbf{\Psi}(\mathbf{x}_j))^H (\mathbf{\Psi}(\mathbf{x}_i) - \mathbf{\Psi}(\mathbf{x}_j))$ on the S-to-R link, respectively. Next, on the R-to-D link, $P_b(R \to D)$ is bounded as

$$P_b(R \to D) \leq \frac{1}{Cb\varepsilon_x} \sum_i \sum_{j,j \neq i} d_H(\hat{\mathbf{x}}_i, \hat{\mathbf{x}}_j) P_{RD}(\hat{\mathbf{x}}_i \to \hat{\mathbf{x}}_j), \tag{16}$$

where $P_{RD}(\hat{\mathbf{x}}_i \to \hat{\mathbf{x}}_j)$ is the PEP between symbol matrices $\hat{\mathbf{x}}_i$ and $\hat{\mathbf{x}}_j$. Following similar steps from (13)-(14), we obtain

$$P_{RD}(\hat{\mathbf{x}}_i \to \hat{\mathbf{x}}_j) \leq \left(\frac{1}{\prod_{l=1}^{r_{rd}} (1 + \frac{\gamma_r \lambda_{rd}^{lij}}{4L_{rd}})} \right), \tag{17}$$

where r_{rd} and λ_{rd}^{lij} are the rank and eigenvalue of $(\mathbf{\Psi}(\mathbf{x}_i) - \mathbf{\Psi}(\mathbf{x}_j))^H (\mathbf{\Psi}(\mathbf{x}_i) - \mathbf{\Psi}(\mathbf{x}_j))$ on the R-to-D link, respectively, γ_r is the normalized SNR on the R-to-D link. From (11), (15), (17), we have

$$\begin{aligned} P_b \;\leq\; & \frac{1}{Cb\varepsilon_x} \sum_i \sum_{j,j \neq i} d_H(\mathbf{x}_i, \mathbf{x}_j) \left(\frac{1}{\prod_{l=1}^{r_{sr}} (1 + \frac{\gamma_s \lambda_{sr}^{lij}}{4L_{sr}})} \right) \\ & + \frac{1}{Cb\varepsilon_x} \sum_i \sum_{j,j \neq i} d_H(\hat{\mathbf{x}}_i, \hat{\mathbf{x}}_j) \left(\frac{1}{\prod_{l=1}^{r_{rd}} (1 + \frac{\gamma_r \lambda_{rd}^{lij}}{4L_{rd}})} \right). \end{aligned} \tag{18}$$

At high SNRs, using the approximation $(1 + \frac{\gamma_s}{4L_{sr}}) \approx (\frac{\gamma_s}{4L_{sr}})$ and $(1 + \frac{\gamma_r}{4L_{rd}}) \approx (\frac{\gamma_r}{4L_{rd}})$, (18) can be written as

$$P_b \leq \tilde{C}_1 \gamma_s^{-r_{sr}} + \tilde{C}_2 \gamma_r^{-r_{rd}}, \tag{19}$$

where $\tilde{C}_1 = \frac{1}{Cb\varepsilon_x} \sum_i \sum_{j,j \neq i} d_H(\mathbf{x}_i, \mathbf{x}_j) \left(\prod_{l=1}^{r_{sr}} (\frac{\lambda_{sr}^{lij}}{4L_{sr}}) \right)$ and $\tilde{C}_2 = \frac{1}{Cb\varepsilon_x} \sum_i \sum_{j,j \neq i} d_H(\hat{\mathbf{x}}_i, \hat{\mathbf{x}}_j) \left(\prod_{l=1}^{r_{rd}} (\frac{\lambda_{rd}^{lij}}{4L_{rd}}) \right)$ are appro-

priately defined constants. For equal power allocation at S and R, we have $\gamma_s = \gamma_r = \gamma$. So, (19) becomes

$$P_b \leq \tilde{C}_1 \gamma^{-r_{sr}} + \tilde{C}_2 \gamma^{-r_{rd}}. \tag{20}$$

For $r_{sr} \gg r_{rd}$, at high SNRs, the second term in (20) dominates. Therefore, (20) can be written as

$$P_b \leq \tilde{C}_2 \gamma^{-r_{rd}}. \tag{21}$$

Therefore, the diversity order is r_{rd}. On the other hand, for $r_{sr} \ll r_{rd}$, the first term in (20) dominates and the diversity order is r_{sr}. Combining these two, the diversity order can be written as $\min\{r_{sr}, r_{rd}\}$. The above diversity order can be generalized for as follows.

- For the system without PR, the achieved diversity order is $\min\{r_{sr}, r_{rd}\}$, where $r_{sr} \leq L_{sr}$ and $r_{rd} \leq L_{rd}$.
- For the system with PR, the achieved diversity order is $\min\{L_{sr}, L_{rd}\}$, since $r_{sr} = L_{sr}$ and $r_{rd} = L_{rd}$.

IV. Results and Discussions

In this section, we present simulation results to validate the diversity analysis previously discussed. We evaluate the bit error rate (BER) performance of the OTFS-IM system with DaF relaying with and without PR. The simulations use a carrier frequency of 4 GHz and a subcarrier spacing of 3.75 kHz. In all the simulations we consider $L = 2, 4$ and various DD profiles (α_i, β_i) used given in Table I.

OTFS-IM with DaF (without PR): Figure 3 shows the simulated BER of OTFS-IM DaF without PR for a frame size of $M = N = 2$, $L_{sr} = 2$, and $L_{rd} = 2$. The information symbols are taken from the BPSK constellation with $u = 4$ bins per SB, and $v = 2$ active bins are considered. In the S-to-R link, DD profile-2 is considered for the simulations, while for the R-to-D link, both DD profiles 1 and 2 are considered. The simulation results show a diversity slope of one for the system that uses DD profile-1 in the R-to-D link, where the achieved diversity is the minimum rank of the two links, which is one in this case. On the other hand, the system that employs DD profile-2 in both links exhibits a diversity slope of two, since the minimum rank is two in this case. Further, the theoretical upper bounds gradually approach the simulation results, validating the analysis.

OTFS-IM with DaF (without and with PR): Figure 4 shows the simulated BER of OTFS-IM with DaF, with and without PR, for $M = 4$, $N = 2$, $L_{sr} = 2, 4$, $L_{rd} = 2, 4$, $u = 8$, $v = 3$, BPSK modulation, and ML detection. The simulation uses DD profiles 3, 4, and 5, as given in Table I. For the system with $L_{sr} = L_{rd} = 2$, DD profile-3 is used in the S-to-D link, and DD profile-4 is used in the R-to-D link. From the simulation, the observed diversity is 1 without PR and 2 with PR. This aligns with the analysis, where the diversity without PR is $\min\{r_{sr}, r_{rd}\} = 1$, since $r_{sr} = 2$ and $r_{rd} = 1$, and with PR it is $\min\{L_{sr}, L_{rd}\} = 2$, validating the analysis.

For the system with $L_{sr} = L_{rd} = 4$, DD profile-5 is used in both the links, and the observed diversity without PR is 2, aligning with the minimum rank of 2 obtained from Table I, thus validating the analysis. However, when subjected to PR, the observed diversity order is 4. This also aligns with the analysis, which indicated a diversity order of $\min\{r_{sr}, r_{rd}\} = 4$, since $r_{sr} = r_{rd} = 4$.

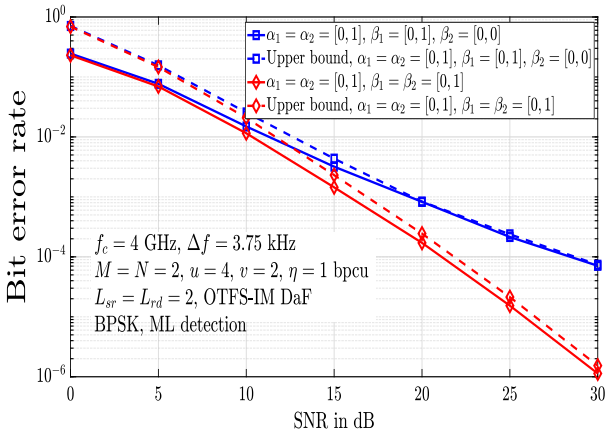

Fig. 3: Bit error rate performance of OTFS-IM with DaF without PR for $M = N = 2$, $L_{sr} = 2$, $L_{rd} = 2$.

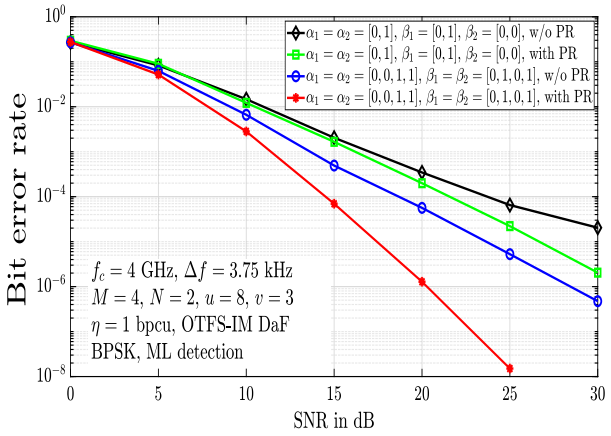

Fig. 4: Bit error rate performance of OTFS-IM with DaF without and with PR for $M = 4$, $N = 2$, $L_{sr} = 2, 4$, $L_{rd} = 2, 4$.

Performance for large (M, N) values: In Fig. 5, we demonstrate the BER performance of OTFS DaF with and without indexing, utilizing system parameters according to the IEEE 802.11p standard [20]. The system operates at a carrier frequency of 5.9 GHz with a subcarrier spacing of 0.156 MHz. A frame size of $M = 64$ and $N = 12$ is employed for the simulations, along with $L_{sr} = L_{rd} = 8$ DD paths. Fractional DDs are used with a maximum speed of 220 km/h, corresponding to a maximum Doppler of 1.2 kHz. The system uses 4-QAM modulation with $u = 4$, $v = 1$ and MMSE detection. With the above parameters, the achieved rate with indexing is 1 bpcu. We compare the performance of this system with a system without indexing with BPSK whose rate is 1 bpcu. From the simulation results, it is evident that OTFS DaF with IM outperforms OTFS DaF without IM. At a BER of 10^{-4}, OTFS-IM with DaF shows an approximate gain of 2.2 dB over OTFS DaF without IM.

Performance comparison between OTFS-IM DaF and

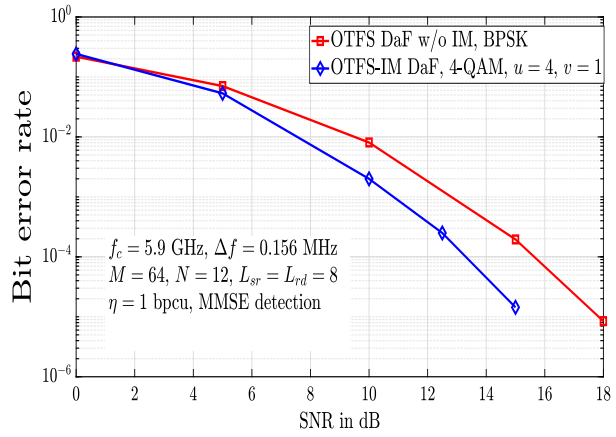

Fig. 5: BER performance of OTFS DaF without and with indexing for $M = 64$, $N = 12$, and $L_{sr} = L_{rd} = 8$.

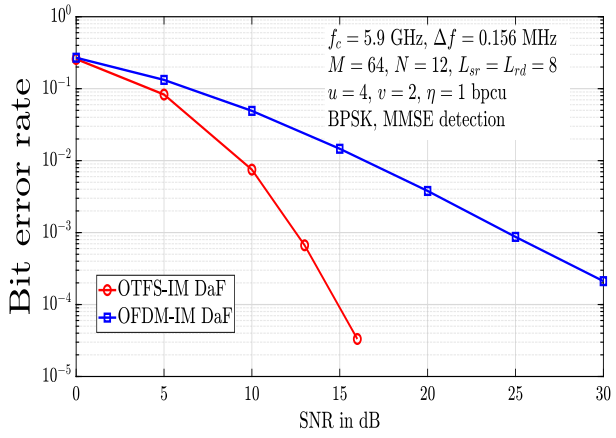

Fig. 6: BER performance of OTFS-IM DaF and OFDM-IM DaF for $M = 64$, $N = 12$, and $L_{sr} = L_{rd} = 8$.

OFDM-IM DaF: In Fig. 6, a performance comparison is presented between OTFS-IM and OFDM-IM with DaF. Both systems are evaluated based on the IEEE 802.11p standard [20] and utilize fractional DDs with a maximum speed of 220 km/h (corresponding to a maximum Doppler of 1.2 kHz). The simulation includes $L_{sr} = L_{rd} = 8$ DD paths, $u = 4$ and $v = 2$, and employs BPSK modulation with MMSE detection. The results demonstrate the superior performance of OTFS-IM with DaF compared to OFDM-IM with DaF. Specifically, at a BER of 10^{-3}, OTFS-IM with DaF exhibits an approximate gain of 12 dB over OFDM-IM with DaF.

V. Conclusions

We examined the performance of the OTFS-IM system with decode and forward relaying. We considered a single relay to aid the communication between the transmitter and receiver. We derived a closed-form expression for the end-to-end PEP in this system and assessed the achieved asymptotic diversity order with and without PR. Our simulation results showed that the use of indexing improves the performance of OTFS with decode and forward relaying, validating the analytically derived diversity orders. Future works can include the diversity analysis of OTFS-IM with DaF relaying for multiple antennas at the transmitter and receiver, investigating optimal power allocation schemes for the source and relay nodes, exploring the impact of multiple relay nodes with relay selection, and analyzing the effect of inter-node distances on the achieved diversity performance.

References

[1] R. Hadani *et al.*, "Orthogonal time frequency space modulation," *Proc. IEEE WCNC'2017*, pp. 1-7, Mar. 2017.

[2] S. S. Das, R. Prasad, *OTFS: Orthogonal Time Frequency Space Modulation - A Waveform for 6G*, River Publishers, 2022.

[3] Y. Hong, T. Thaj, and E. Viterbo, *Delay-Doppler Communications: Principles and Applications*, Academic Press, 2022.

[4] P. Raviteja, K. T. Phan, Y. Hong, and E. Viterbo, "Interference cancellation and iterative detection for orthogonal time frequency space modulation," *IEEE Trans. Wireless Commun.*, vol. 17, no. 10, pp. 6501-6515, Aug. 2018.

[5] H. Qu, G. Liu, L. Zhang, S. Wen, and M. A. Imran, "Low-complexity symbol detection and interference cancellation for OTFS system," *IEEE Trans. Commun.*, vol. 69 no. 3, pp. 1524 - 1537, Dec. 2020.

[6] G. D. Surabhi, R. M. Augustine, and A. Chockalingam, "On the diversity of uncoded OTFS modulation in doubly-dispersive channels," *IEEE Trans. Wireless Commun.*, vol. 18, no. 6, pp. 3049-3063, Jun. 2019.

[7] P. Raviteja, Y. Hong , E. Viterbo , and E. Biglieri, "Effective diversity of OTFS modulation," *IEEE Wireless Commun. Lett.*, vol. 9, no. 2, pp. 249-253, Feb. 2020.

[8] V. S. Bhat, G. D. Surabhi, and A. Chockalingam, "Performance analysis of OTFS modulation with receive antenna selection," *IEEE Trans. Veh. Tech.*, vol. 70, no. 4, pp. 3382-3395, Apr. 2021.

[9] S. Li, J. Yuan, W. Yuan, Z. Wei, B. Bai, and D. W. K. Ng, "Performance analysis of coded OTFS systems over high-mobility channels," *IEEE Trans. Wireless Commun.*, vol. 20, no. 9, pp. 6033-6048, Sep. 2021.

[10] Y. Liang, L. Li, P. Fan, and Y. Guan, "Doppler resilient orthogonal time-frequency space (OTFS) systems based on index modulation," *Proc. IEEE VTC'2020-Spring*, pp. 1-5, May-Jul. 2020.

[11] J. K. Francis, R. M. Augustine, and A. Chockalingam, "Diversity and PAPR enhancement in OTFS using indexing," *Proc. IEEE VTC'2021*, May 2021.

[12] H. Zhao, D. He, Z. Kang, and H. Wang, "Orthogonal time frequency space (OTFS) with dual-mode index modulation," *IEEE Wireless Commun. Lett.*, vol. 10, no. 5, pp. 991-995, May 2021.

[13] D. Feng, J. Zheng, B. Bai, J. Jiang, and L. Zheng, "In-phase and quadrature index modulation aided OTFS transmission," *IEEE Commun. Lett.*, vol. 26, no. 6, pp. 1318-1322, Jun. 2022.

[14] J. N. Laneman, D. N. C. Tse, and G. W. Wornell, "Cooperative diversity in wireless networks: Efficient protocols and outage behavior," *IEEE Trans. Inform. Theory*, vol. 50, no. 12, pp. 3062-3080, Dec. 2004.

[15] A. Nosratinia, T. E. Hunter, and A. Hedayat, "Cooperative communication in wireless networks," *IEEE Commun. Mag.*, vol. 42, no. 10, pp. 74-80, Oct. 2004.

[16] M. O. Hasna and M.-S. Alouini, "End-to-end performance of transmission systems with relays over Rayleigh-fading channels," *IEEE Trans. Wireless Commun.*, vol. 2, no. 6, pp. 1126-1131, Nov. 2003.

[17] Y. Khattabi and M. M. Matalgah, "Conventional and best-relay-selection cooperative protocols under nodes-mobility and imperfect-CSI impacts: BER performance," *Proc. IEEE WCNC'2015*, pp. 105-110, May 2015.

[18] N. Varshney and A. K. Jagannatham, "Performance analysis of MIMO-OSTBC based selective DF cooperative wireless system with node mobility and channel estimation errors," *Proc. Nat. Conf. Commun.*, pp. 1-6, IIT Guwahati, Mar. 2016.

[19] J. Shi, J. Hu, Y. Yue, X. Xue, W. Liang and Z. Li, "Outage probability for OTFS based downlink LEO satellite communication," *IEEE Trans. Veh. Tech.*, vol. 71, no. 3, pp. 3355-3360, March 2022.

[20] A. M. S. Abdelgader and W. Lenan, "The physical layer of the IEEE 802.11p WAVE communication standard: the specifications and challenges," *Proc. World Congr. Eng. Comput. Sci.*, pp. 22-24, Oct. 2014.